

## NANO EXPRESS

## Open Access



# Synthesis and Electrochemical Property of $\text{LiMn}_2\text{O}_4$ Porous Hollow Nanofiber as Cathode for Lithium-Ion Batteries

Lianfeng Duan<sup>1,2</sup>, Xueyu Zhang<sup>1,2</sup>, Kaiqiang Yue<sup>1,2</sup>, Yue Wu<sup>1,2</sup>, Jian Zhuang<sup>3</sup> and Wei Lü<sup>1,2\*</sup>

## Abstract

The  $\text{LiMn}_2\text{O}_4$  hollow nanofibers with a porous structure have been synthesized by modified electrospinning techniques and subsequent thermal treatment. The precursors were electrospun directly onto the fluorine-doped tin oxide (FTO) glass. The heating rate and FTO as substrate play key roles on preparing porous hollow nanofiber. As cathode materials for lithium-ion batteries (LIBs),  $\text{LiMn}_2\text{O}_4$  hollow nanofibers showed the high specific capacity of 125.9 mAh/g at 0.1 C and a stable cycling performance, 105.2 mAh/g after 400 cycles. This unique structure could relieve the structure expansion effectively and provide more reaction sites as well as shorten the diffusion path for  $\text{Li}^+$  for improving electrochemical performance for LIBs.

**Keywords:**  $\text{LiMn}_2\text{O}_4$ , Porous structure, Hollow nanofibers, Cathodes, Lithium-ion batteries

## Background

Lithium-ion battery (LIB) as energy storage devices is widely considered as the most promising rechargeable power sources because of high power density, no memory effect, long cycle life, high voltage, and low self-discharge, expecting to be utilized in portable electronic appliances and electric vehicles (EVs) [1, 2]. To improve the energy density and cycle performance of LIBs, much more efforts have been made to develop the new electrode materials, especially for cathode [3, 4]. The composition  $\text{LiM}_x\text{O}_y$  ( $M = \text{Co}, \text{Ni}, \text{V}, \text{Si}, \text{etc.}$ ) has attracted much attention as high-energy density cathode materials for lithium rechargeable batteries [5–7]. Among different kinds of cathode materials for lithium battery,  $\text{LiMn}_2\text{O}_4$  is considered to be an attractive cathode material because of its low cost, abundant resources, low toxicity, and better safety, compared to other transition metal oxides [8, 9]. Wang et al. fabricated  $\text{LiMn}_2\text{O}_4$  nanofiber with a specific capacity of 110 mAh/g at 0.5 C after 60 cycles [10]. In addition, Kanamura et al. prepared

$\text{LiMn}_2\text{O}_4$  thin film by the PVP sol-gel method and the capacity fade was ca. 20% during 200 cycles [11]. However, due to the dissolution of Mn ion into the electrolyte and structural distortion, it suffers capacity fading on cycling resulting in a poor long-term cycle stability [12, 13].

The cathode materials with special structure and morphology could increase their specific capacity and cycling performance, aiming to overcome the mechanical strain arising from the huge volume variation and the particle agglomerations during the charge/discharge processes of lithium-ion battery, which results in the increased diffusion lengths and serious electrical disconnection [3, 14, 15]. The porous structure can buffer the large volume change and the agglomerations of electrode, which could be enhanced the cycling performance [16, 17]. So, one-dimensional (1D) nanofibers with porous structure have been demonstrated to be the new structure cathode for LIBs [18]. Because of its simple procedure and good controllability, the electrospinning technique is appealing in synthesizing nanofibers compared with other methods, such as chemical vapor deposition, pulsed laser deposition, hydrothermal process, sol-gel methods [19–21].

In this work,  $\text{LiMn}_2\text{O}_4$  nanofiber with porous hollow structure and morphology has been successfully

\* Correspondence: [lw771119@hotmail.com](mailto:lw771119@hotmail.com)

<sup>1</sup>Advanced Institute of Materials Science, Key Laboratory of Advanced Structural Materials, Ministry of Education, Changchun University of Technology, Changchun 130012, China

<sup>2</sup>Department of Materials Science and Engineering, Changchun University of Technology, Changchun 130012, China

Full list of author information is available at the end of the article

synthesized by modified electrospinning method. It is discussed that the effects of varied heat treatment factors in detail which explore the formation mechanism of nanofibers with a hollow structure. Furthermore, the electrochemical performances of the samples as cathode for LIBs were evaluated. It is worth that  $\text{LiMn}_2\text{O}_4$  porous hollow nanofiber morphology delivers the higher electrochemical performance.

## Methods

### Preparation of $\text{LiMn}_2\text{O}_4$ Nanofibers

The  $\text{LiMn}_2\text{O}_4$  nanofiber with porous hollow structure and morphology has been successfully synthesized by modified electrospinning method. All chemicals were of analytical grade and used as purchased without further purification. Firstly, the precursor solution was prepared by mixing 2 g of polyvinylpyrrolidone (PVP,  $M_w \approx 1,300,000$ ) in 20 ml ethanol under vigorous stirring for 4 h. 1.224 g  $\text{Li}(\text{CH}_3\text{COO}) \cdot 2\text{H}_2\text{O}$  and 5.88 g  $\text{Mn}(\text{CH}_3\text{COO})_2 \cdot 4\text{H}_2\text{O}$  were dissolved into the solution. And the acetic acid (1 ml) was then added to the above solution under continuous stirring for 2 h. After that, the precursor solution was transferred into a syringe with the metal syringe needle. The 20 kV high voltage was applied across the collector (aluminum foil or fluorine-doped tin oxides (FTOs)) and metal needle, whose distance maintained at 20 cm. The precursor collected on collectors was dried at 60 °C for 1 h.  $\text{LiMn}_2\text{O}_4$  cathode was obtained by calcining the precursor nanofibers in air under different heating rates and temperatures.

### Materials Characterization

The X-ray diffraction patterns (XRD) of fabricated powders were recorded by a Rigaku D/max 2500 pc X-ray diffractometer with Cu K radiation ( $\lambda = 1.54156 \text{ \AA}$ ) at a scan rate of 5 deg/s. The field emission scanning electron microscope (FESEM) was conducted on a JEOL JSM-6700F field emission scanning electron microscopy. Transmission electron microscopy (TEM) and high-resolution TEM (HRTEM) observations were performed by a JEOL 2100F. The thermogravimetric (TG) curves were obtained by a Perkin-Elmer TGA 7 thermogravimetric analyzer from room temperature to 800 °C at a heating rate of 10 °C/min. Brunauer-Emmett-Teller (BET)  $\text{N}_2$  adsorption-desorption surface area measurements were conducted on a volumetric sorption analyzer (NOVA 2000, Quantachrome).

### Electrochemical Property

The electrochemical experiments of  $\text{LiMn}_2\text{O}_4$  nanofiber with porous hollow structure for the working electrode, which prepared by casting slurry containing 10% acetylene black, 10% polyvinylidene fluoride (PVDF), and 80% active material onto a aluminum foil, were performed

via CR2025-type coin cells assembled in a dry argon-filled glove box. The test cell was assembled using working electrode and lithium foil which were separated by a Celgard 2400 microporous membrane. The electrolyte solution was prepared by dissolving 1 M  $\text{LiPF}_6$  in ethyl carbonate and diethyl carbonate (1:1 by volume). Galvanostatic charge-discharge cycling tests were performed using a LAND CT2001A multi-channel battery testing system in the voltage range between 3.0 and 4.4 V at room temperature.

## Results and Discussion

Figure 1a, b shows the FESEM images of precursor nanofibers and the  $\text{LiMn}_2\text{O}_4$  nanofibers annealed at 700 °C for 5 h with a heating rate of 5 °C/min, respectively. Figure 1a shows the morphology of precursor nanofiber, which exhibits smooth surface. The diameter of nanofiber is about 500 nm. After thermal treatment, the nanofiber has been formed with uniform diameter of about 200 nm and porous surface because of the burnout of organic components during the calcination process (as shown in Fig. 1b). In addition, the nanofibers form “network” structures, which facilitate the fast charge-discharge characteristics, because the structure could provide short lithium diffusion path and large surface area [10]. Figure 1c shows the hollow structure of nanofibers, which is clearly from the inset of Fig. 1c. The thickness of the tube wall is about 50 nm and the diameter of hollow structure is about 80 nm (Fig. 1d). From the HRTEM image (Fig. 1e), the lattice fringe spacing of the  $\text{LiMn}_2\text{O}_4$  particles is almost in accordance with the d-spacing value (4.76 Å) of cubic  $\text{LiMn}_2\text{O}_4$  in (111) plane. And the regular lattice fringes can also demonstrate the high crystallinity [22, 23]. Figure 1f shows the selected area electron diffraction (SAED) pattern; it indicates that the nanofibers are single crystalline and the corresponding miller indices are indexed accordingly [24].

Figure 2a is the FESEM of the  $\text{LiMn}_2\text{O}_4$  nanoparticles calcined at 650 °C and 5 °C/min, the particles with heterogeneous size could be prepared, without nanofibers. Figure 2b is the X-ray diffraction pattern of the  $\text{LiMn}_2\text{O}_4$  nanofibers calcined at different temperatures. As it can be seen from Fig. 2b, the diffraction peaks (calcined at 700 °C) can be indexed to  $\text{LiMn}_2\text{O}_4$  phase (JCPDS 88-1749) with no other impurities. Meanwhile, the sharpness of the X-ray diffraction peaks confirms that the material should be crystallized  $\text{LiMn}_2\text{O}_4$ . However, some peaks which belong to  $\text{Mn}_2\text{O}_3$  phase are also can be seen in the nanofibers obtained at 650 °C, which is evident that the presence of unavoidable impurity phase ( $\text{Mn}_2\text{O}_3$ ) is can be seen when the as-spun  $\text{LiMn}_2\text{O}_4$  nanofibers are treated at a temperature of 650 °C [25]. The calcination and the decomposition temperature of

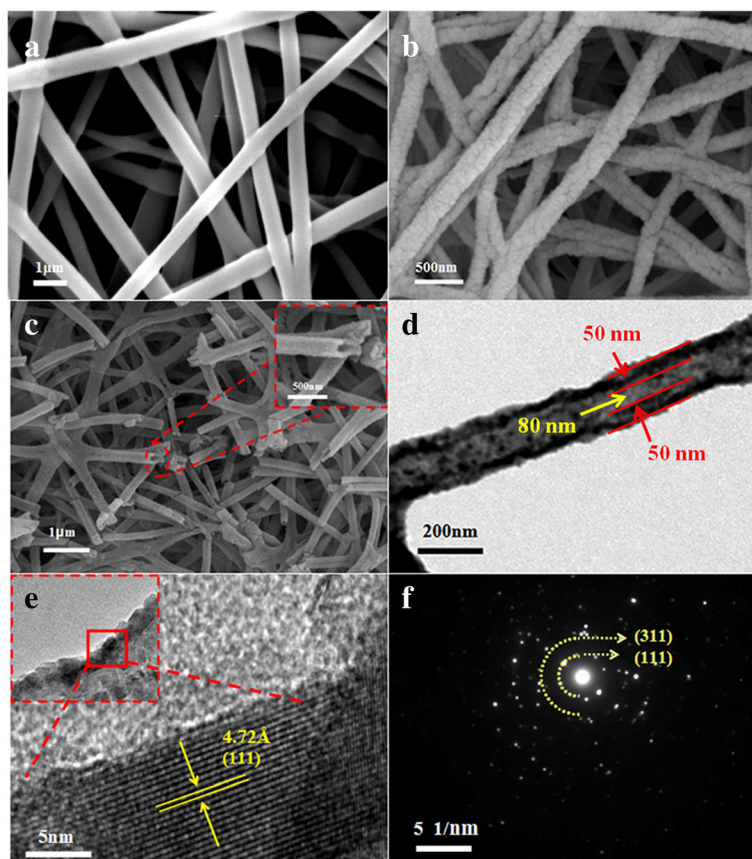


**Fig. 1** **a** FESEM image of electrospun  $\text{LiMn}_2\text{O}_4$  nanofibers precursor. **b**  $\text{LiMn}_2\text{O}_4$  nanofibers after being annealed at 700 °C for 5 h. **c** Nanofibers with a hollow structure (*Inset* magnified view of nanofibers indicating hollow structure), **d** TEM image, **e** HRTEM image, **f** SAED image of porous hollow nanofiber

precursor were determined by thermogravimetric (TG) analysis. In Fig. 3, the first weight loss (0–130 °C) could be resulted from the evaporation of hydrate. Then, a noticeable weight loss (36.6 wt% of original weight) is observed between 250 and 450 °C because of the decomposition of PVP. So, the pre-heated temperature is at 500 °C for removing the PVP completely. From above, the  $\text{LiMn}_2\text{O}_4$  nanofibers without any other impurities could be synthesized at 700 °C.

To understand the formation mechanism of the porous hollow nanofibers structure, the as-prepared samples were analyzed by FESEM at different heating rates (3, 5, and 7 °C/min) with different substrates such as Al foil (a, b, c) and FTO (d, e, f) in Fig. 4. In this figure, with increasing the heating rate from 3 °C/min to 5 °C/min, the size of nanoparticles and diameter of nanofibers are decreased, and then, they are increased from 5 °C/min to 7 °C/min. At the high-temperature heating (7 °C/

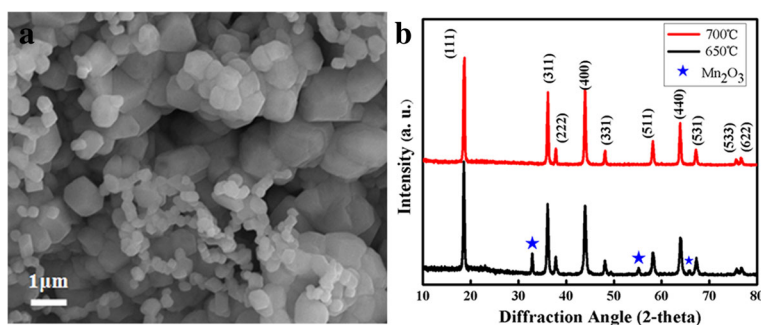
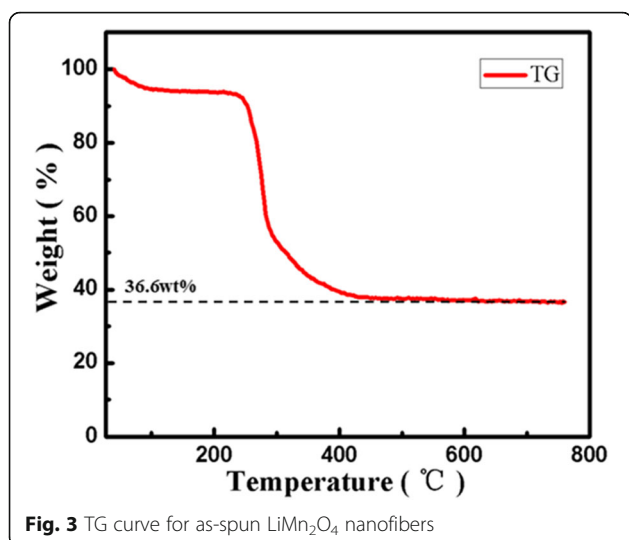


**Fig. 2** **a** FESEM images of samples calcined at 650 °C, **b** X-ray diffraction pattern of calcined  $\text{LiMn}_2\text{O}_4$  nanofibers at 650 and 700 °C



min), the highly porous structure should be destroyed to create a dense morphology for use in Li-ion batteries. Therefore, the porous hollow wires in this process are ideal for obtaining highly crystalline nanomaterials to be used as the active material at 5 °C/min. First of all, at the slow heating rate was employed, the decomposition of polymer and the release of  $\text{CO}_2$  and  $\text{H}_2\text{O}$  are slower, so the  $\text{LiMn}_2\text{O}_4$  particles formed earlier have more time to grow. Following it, the size of nanoparticles is larger and the morphologies of the samples are bending and rough because of the quickly decomposition of polymer and growth of crystal. It is shown that the morphology of porous surface is affected by the higher release of  $\text{CO}_2$  and  $\text{H}_2\text{O}$  with the higher heating rate. In addition, the porous hollow nanofibers could be more synthesis on FTO as substrate. The agglomeration of nanofibers is much more serious with Al foil as substrate in Fig. 4. Compared to

Al foil, the FTO is a kind of semiconductors as transparent conducting oxide with higher resistivity, stable chemical performance, and strong acid and alkali resistance at room temperature. Just for it, at the same voltage for applying across the collector and metal needle, the jet velocity of the precursor solution is slower than that of the Al foil. The fiber morphology of the precursor collected on FTO could be kept more integrity and uniformity. The FTO could be used for substrate at the electrospinning process. So, we first prepared the  $\text{LiMn}_2\text{O}_4$  porous hollow nanofibers by electrospinning it onto FTO glass directly to form porous electrode.

The formation of the hollow nanofibers with porous structure is introduced in Fig. 5. There are three stages for the formation process of unique structure: (1) The precursor nanofibers are prepared on the FTO by electrospinning. (2) Under thermal treatment, the polymer at the surface of precursor nanofibers decomposes into  $\text{H}_2\text{O}$  and  $\text{CO}_2$  and releases, meanwhile the inner organic moieties together with metal ions present in the precursor move toward the outer wall under the effect of concentration difference [26]. In that case, the gas diffusion rate from the interspaces between the nanoparticles is slower than that of PVP decomposition, which makes the pressure inside of the composite fibers larger than that outside of the composite fibers, and the nanoparticles would move toward outside of the composite fibers to form hollow fibers. (3) With the temperature further increasing, the  $\text{Li}^+$  and  $\text{Mn}^{2+}$  aggregated react with each other in the air atmosphere resulting in the formation of  $\text{LiMn}_2\text{O}_4$ , which continues to grow and interconnects to form the final continuous tubular structure with porous and thin wall [27, 28]. The formation mechanism of hollow nanofibers and the key roles of FTO as substrate need to be further studied in the future. It is also the

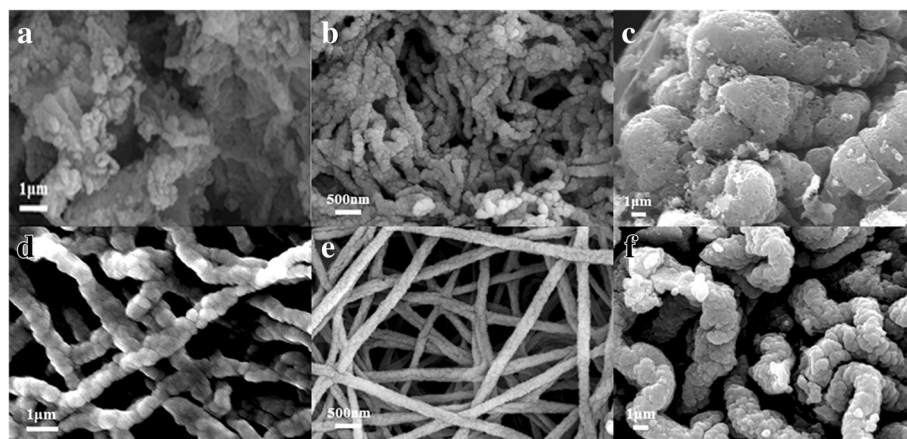
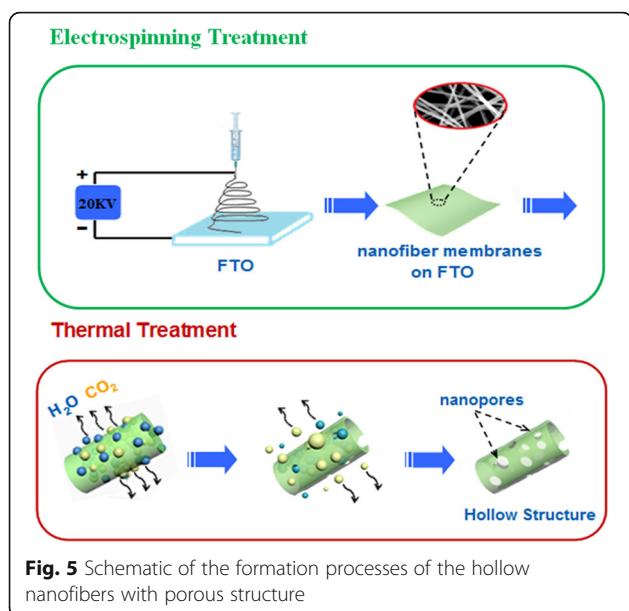


**Fig. 4** FESEM images of samples after being calcinated at different heating rates **a, d** 3 °C/min, **b, e** 5 °C/min, **c, f** 7 °C/min with Al foil (**a, b, c**) and FTO (**d, e, f**)





base of synthesizing the nanofiber composites as cathode for LIBs.

N<sub>2</sub> adsorption-desorption and the corresponding pore size distribution curve of S1, S2, and S3 LiMn<sub>2</sub>O<sub>4</sub> nanofibers (heating rates are 3, 5, and 7 °C/min, respectively) are shown in Fig. 6. Figure 6a shows the large hysteresis loops between the N<sub>2</sub> adsorption and desorption isotherms in the  $P/P_0$  ranging from 0.7 to 1. It confirms the broad pore size distribution toward larger mesopores (inset of Fig. 6) and the formation of mesopore textural porosity. The BET specific surface area of S2 is 84.3 m<sup>2</sup>/g, and the average pore size is around 60 nm, which are in good agreement with the TEM analysis. However, the BET specific surface areas and pore sizes of S1 and S3 are much smaller than S2. The larger mesopore derives from the gas diffusion decomposed from PVP, which drives the nanoparticles to transfer from interior to exterior of the composite fibers.

The electrochemical performances of the LiMn<sub>2</sub>O<sub>4</sub> porous hollow nanofibers (S2) were evaluated by galvanostatic

charge/discharge cycling in the voltage range of 3.0–4.4 V at 0.1 C (1 C = 148 mAh/g). In Fig. 7a, there are two distinct voltage plateaus at 4.1 and 4.0 V, respectively, corresponding to the two-step intercalation and deintercalation of Li<sup>+</sup> into or out LiMn<sub>2</sub>O<sub>4</sub> during the charge and discharge process. The two flat voltage plateaus are corresponding to the two-phase and one-phase reaction modes, respectively, which are the region equilibrium between LiMn<sub>2</sub>O<sub>4</sub> and Li<sub>0.5</sub>Mn<sub>2</sub>O<sub>4</sub> phases ( $\text{LiMn}_2\text{O}_4 \rightleftharpoons \text{Li}_{0.5}\text{Mn}_2\text{O}_4 + 0.5\text{Li}^+ + 0.5\text{e}^-$ ) and the equilibrium between Li<sub>0.5</sub>Mn<sub>2</sub>O<sub>4</sub> and  $\gamma\text{-MnO}_2$  ( $\text{Li}_{0.5}\text{Mn}_2\text{O}_4 \rightleftharpoons 2\text{MnO}_2 + 0.5\text{Li}^+ + 0.5\text{e}^-$ ) [29]. The electrode exhibits a discharge capacity of 125.9 mAh/g and charge capacity of 132.8 mAh/g at 0.1 C for the first cycle. The well overlapping of charge-discharge curves and the mild capacity fading between 1 and 10 cycles indicate that there is less severe formation of SEI films and polarization effect occurs during the circulation [30]. After 100 and 200 cycles, it still retains a capacity of 117.2 and 114.9 mAh/g, which decreases slightly. Similar trend is observed at 0.5 C and 1 C, reaching a specific capacity of 115 and 103.8 mAh/g after 200 cycles, respectively (Fig. 7b). Figure 7c shows the exceedingly stable long-term cycling performance of the LiMn<sub>2</sub>O<sub>4</sub> porous hollow nanofibers, which shows the capacity remains of 105.2 mAh/g at 0.1 C after 400 cycles. As it can be seen from Fig. 7c inset, there are also two distinct separated voltage plateaus. It is evidenced that the porous hollow nanofibers possess an outstanding structure and component stability during charge-discharge process.

Figure 8a presents the rate capability of the LiMn<sub>2</sub>O<sub>4</sub> hollow nanofibers. The LiMn<sub>2</sub>O<sub>4</sub> electrode shows a capacity loss from 122 mAh/g at 0.1 C to 102 mAh/g at 1 C, which is only 16.3% of an initial discharge capacity at 0.1 C. Furthermore, after 80 cycles (from the 81st cycle to the 161st cycle), the discharge capacity of LiMn<sub>2</sub>O<sub>4</sub> could be recovered (123 mAh/g), when the charge-discharge rates reduce from 1 C to 0.1 C. Figure 8b shows the cycling performance of the S1, S2, and S3 with different morphologies at a current rate of 0.1 C. The S2 (Fig. 4e) electrode delivers an initial

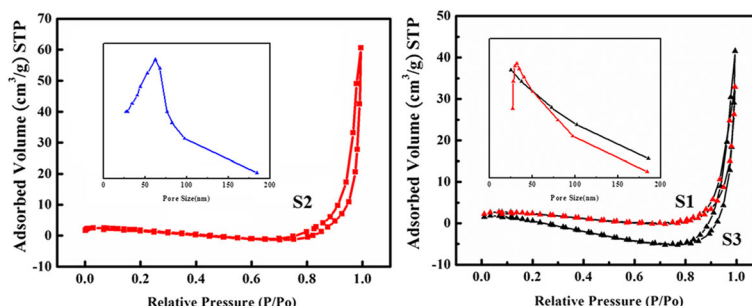


**Fig. 6** N<sub>2</sub> adsorption-desorption isotherms for LiMn<sub>2</sub>O<sub>4</sub> nanofibers S2 (a), S1 and S3 (b), with insets showing the BJH pore size distributions for the corresponding samples

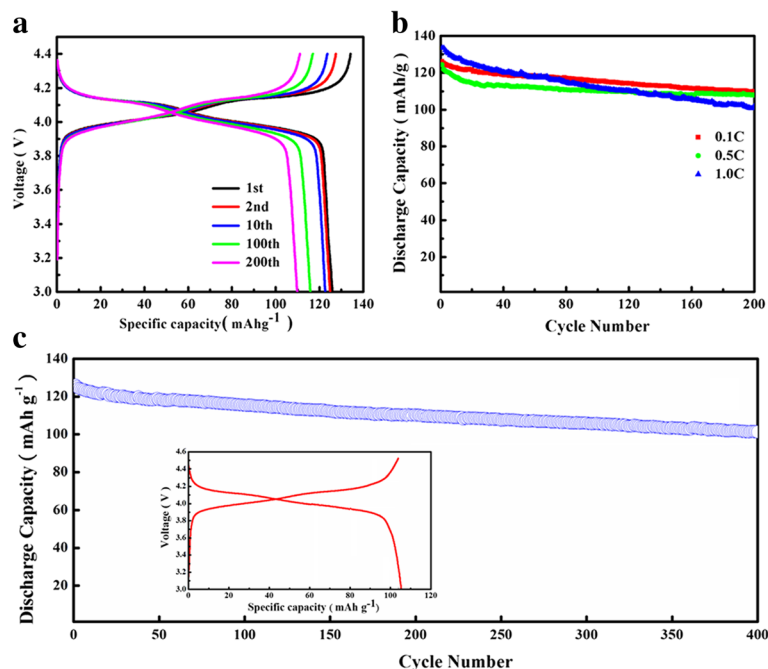


**Fig. 7** **a** Galvanostatic charge-discharge curves of S2 at the current density 0.1 C and **b** cycle performance of S2 at 0.1 C, 0.5 C, and 1.0 C, **c** cycling performance of S2 for 400 cycles at 0.1 C. *Inset* shows the charge-discharge curves of the 400th cycle

discharge capacity of 121 mAh/g. After 200 cycles, the capacity retention is 107 mAh/g. Compared to S1 and S2, S3 shows an initial discharge capacity of 123 mAh/g and retains 86 mAh/g after 200 cycles, and the capacity retention of 70% is much lower than the S2 electrode. It is worth noting that the LiMn<sub>2</sub>O<sub>4</sub> porous hollow nanofiber electrode delivers the excellent rate capability, especially for showing stable electrochemical property at different current densities.

On the basis of the above results, the high reversible capacity, rate behavior, and excellent cycling life of the LiMn<sub>2</sub>O<sub>4</sub> porous hollow nanofibers are due to the novel porous hollow structure. Firstly, the porous nanostructure can provide more reaction sites for the intercalation/deintercalation of Li<sup>+</sup> and shorten the diffusion path for Li<sup>+</sup>, leading to the better rate capability [31, 32].

Secondly, the hollow structure with high crystallinity possesses a high structural stability. The manganese could not be dissolved easily from the spinel phase because of the robust structure. Thirdly, the hollow structure could effectively relieve the structural strain and volume change which can be much more helpful for its long-term circulation. All of them contribute to the high reversible capacity, rate capability, and good cycle performance of porous hollow LiMn<sub>2</sub>O<sub>4</sub> nanofibers as the cathode for LIBs.

## Conclusions

In summary, the LiMn<sub>2</sub>O<sub>4</sub> hollow nanofibers with a porous structure have been synthesized by modified electrospinning techniques on the FTO substrate. And the precursor was calcined in air at 700 °C. As the cathode

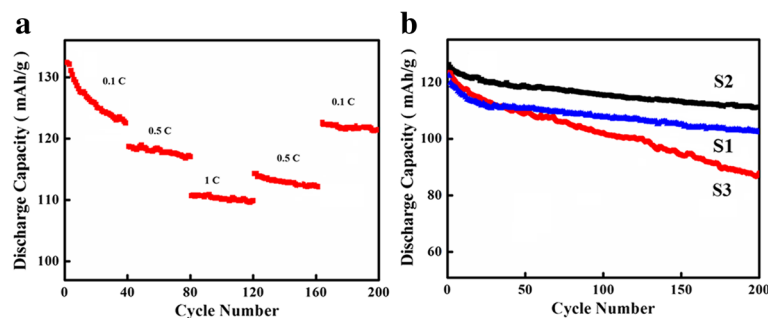


**Fig. 8** **a** Rate performance of S2. **b** Cycling performance of S1, S2, and S3 for 200 cycles at 0.1 C

materials for LIBs, the  $\text{LiMn}_2\text{O}_4$  with special morphology exhibits good cycle life and high capacity, which delivers a high specific capacity of 125.9 mAh/g and a stable cycling performance of 105.2 mAh/g after 400 cycles, at 0.1 C. It is certificated that the porous and hollow structure improves the utilization of the active mass and dual conduction of  $\text{Li}^+$  and electrons and effectively relieves the structural strain and volume change, which could enhance the cycling performance and rate stability for advanced energy storage devices.

#### Abbreviations

LIB: Lithium-ion battery; EV: Electric vehicles; FTO: Fluorine-doped tin oxide; 1D: One-dimensional; PVP: Polyvinylpyrrolidone; XRD: X-ray diffraction patterns; FESEM: Field emission scanning electron microscopy; TEM: Transmission electron microscopy; HRTEM: High-resolution transmission electron microscopy; BET: Brunauer-Emmett-Teller; TG: Thermogravimetric; PVDF: Polyvinylidene fluoride; SAED: Selected area electron diffraction

#### Acknowledgements

The authors thank Dr. Xiaoju Li from the Key Laboratory of Advanced Structural Materials, Ministry of Education, and Department of Materials Science and Engineering, Changchun University of Technology for the TEM characterizations.

#### Funding

This work was supported by the National Nature Science Foundation of China (Grant No. 61574021, No. 61376020, No. 61604017) and the State Scholarship Fund of China Scholarship Council (Grant No. 201408220025).

#### Authors' Contributions

WL and LD conceived the idea. KY and YW carried out the experiments. XZ, JZ, and LD took part in the experiments and the discussion of the results. XZ and LD drafted the manuscript. All authors read and approved the final manuscript.

#### Competing Interests

The authors declare that they have no competing interests.

#### Author details

<sup>1</sup>Advanced Institute of Materials Science, Key Laboratory of Advanced Structural Materials, Ministry of Education, Changchun University of Technology, Changchun 130012, China. <sup>2</sup>Department of Materials Science and Engineering, Changchun University of Technology, Changchun 130012, China. <sup>3</sup>Key Laboratory of Bionics Engineering, Ministry of Education, Jilin University, Changchun 130025, China.

Received: 21 November 2016 Accepted: 31 January 2017

Published online: 10 February 2017

#### References

- Bruce PG, Scrosati B, Tarascon JM (2008) Nanomaterials for rechargeable lithium batteries. *Angew Chem Int Ed* 47:2930
- Park OK, Cho Y, Lee S, Yoo HC, Song HK, Cho J (2011) Who will drive electric vehicles, olivine or spinel? *Energy Environ Sci* 4:1621
- Lin F, Nordlund D, Li YY et al (2016) Metal segregation in hierarchically structured cathode materials for high-energy lithium batteries. *Nature Energy* 1:15004
- Wang YJ, Zhu B, Wang YM, Wang F (2016) Solvothermal synthesis of  $\text{LiFePO}_4$  nanorods as high-performance cathode materials for lithium-ion batteries. *Ceram Int* 42:10297
- Kalyani P, Kalaiselvi N (2005) Various aspects of  $\text{LiNiO}_2$  chemistry: a review. *Sci Tech Adv Mater* 6:689–703
- Tsuyumoto I, Nakakura Y, Yamaki S (2014) Nanosized-layered  $\text{LiVO}_2$  prepared from peroxo-polyvanadic acid and its electrochemical properties. *J Am Ceram Soc* 97:3374–3377
- Chang CC, Wang CC, Kumta PN (2001) Chemical synthesis and characterization of lithium orthosilicate ( $\text{Li}_4\text{SiO}_4$ ). *Materials and Design* 22: 617–623
- Zhao HY, Liu SS, Liu XQ, Tan M, Wang ZW, Cai Y, Komarneni S (2016) Orthorhombic  $\text{LiMnO}_2$  nanorods as cathode materials for lithium-ion batteries: synthesis and electrochemical properties. *Ceram Int* 42:9319
- Xu XD, Lee SH, Jeong SY, Kim YS, Cho J (2013) Recent progress on nanostructured 4V cathode materials for Li-ion batteries for mobile electronics. *Materials Today* 16:487–495
- Zhou HW, Ding XN, Yin Z et al (2014) Fabrication and electrochemical characteristics of electrospun  $\text{LiMn}_2\text{O}_4$  nanofiber cathode for Li-ion batteries. *Mater Lett* 117:175
- Rho YH, Dokko K, Kanamura K (2006)  $\text{Li}^+$  ion diffusion in  $\text{LiMn}_2\text{O}_4$  thin film prepared by PVP sol-gel method. *J Power Sources* 157:471
- Jiang H, Fu Y, Hu YJ et al (2014) Hollow  $\text{LiMn}_2\text{O}_4$  nanocones as superior cathode materials for lithium-ion batteries with enhanced power and cycle performances. *Small* 10:1096
- Ju BW, Wang XY, Wu C et al (2014) Excellent cycling stability of spherical spinel  $\text{LiMn}_2\text{O}_4$  by  $\text{Y}_2\text{O}_3$  coating for lithium-ion batteries. *J Solid State Electrochem* 18:115
- Zhao HY, Liu SS, Wang ZW, Cai Y, Tan M, Liu XQ (2016)  $\text{LiSi}_x\text{Mn}_{2-x}\text{O}_4$  ( $x < 0.10$ ) cathode materials with improved electrochemical properties prepared via a simple solid-state method for high-performance lithium-ion batteries. *Ceramics International* 42:13442
- Min L, Shailesh K, Yong NH, Li SFT (2011) Carbon nanotube supported  $\text{MnO}_2$  catalysts for oxygen reduction reaction and their applications in microbial fuel cells. *Biosens Bioelectron* 26:4728
- Zhang XY, Sun SH, Sun XJ et al (2016) Plasma-induced, nitrogen-doped graphene-based aerogels for high-performance supercapacitors. *Light: Science & Applications* 5, e16130
- Zhang XY, Ge X, Sun SH QYD, Chi WZ, Chen CD, Lü W (2016) Morphological control of RGO/CdS hydrogels for energy storage. *CrystEngComm* 18:1090
- Niu CJ, Meng JS, Wang XP et al (2015) General synthesis of complex nanotubes by gradient electrospinning and controlled pyrolysis. *Nat Commun* 6:7402
- Song MK, Park S, Alamgir FM, Cho J, Liu M (2011) Nanostructured electrodes for lithium-ion and lithium-air batteries: the latest developments, challenges, and perspectives. *Mater Sci Eng R* 72:203
- Cavaliere S, Subianto S, Savych I, Jones DJ, Roziere J (2011) Electrospinning: designed architectures for energy conversion and storage devices. *Energy Environ Sci* 4:4761
- Zhang CL, Yu SH (2014) Nanoparticles meet electrospinning: recent advances and future prospects. *Chem Soc Rev* 43:4423
- Kim JS, Kim K, Cho W, Shin WH, Kanno R, Choi JW (2012) A truncated manganese spinel cathode for excellent power and lifetime in lithium-ion batteries. *Nano Lett* 12:6358
- Qu QT, Fu LJ, Zhan XY et al (2011) Porous  $\text{LiMn}_2\text{O}_4$  as cathode material with high power and excellent cycling for aqueous rechargeable lithium batteries. *Energy Environ Sci* 4:3985
- Zhou L, Zhou XF, Huang XD et al (2013) Designed synthesis of  $\text{LiMn}_2\text{O}_4$  microspheres with adjustable hollow structures for lithium-ion battery applications. *J Mater Chem A* 1:837
- Wang YH, Jia DS, Peng Z, Xia YY, Zheng GF (2014) All-nanowire based Li-ion full cells using homologous  $\text{Mn}_2\text{O}_3$  and  $\text{LiMn}_2\text{O}_4$ . *Nano Lett* 14:1080
- Aravindan V, Sundaramurthy J, Kumar PS, Shubha N, Ling WC, Ramakrishna S, Madhavi S (2013) A novel strategy to construct high performance lithium-ion cells using one dimensional electrospun nanofibers, electrodes and separators. *Nanoscale* 5:10636
- Arun N, Aravindan V, Jayaraman S et al. (2014) Exceptional performance of high voltage spinel  $\text{LiNi}_{0.5}\text{Mn}_{1.5}\text{O}_4$  cathode in all one dimensional architecture with anatase  $\text{TiO}_2$  anode by electrospinning. *Nanoscale* 6:8926
- Liu J, Liu W, Ji SM, Zhou YC, Hodgson P, Li YC (2013) Electrospun spinel  $\text{LiNi}_{0.5}\text{Mn}_{1.5}\text{O}_4$  hierarchical nanofibers as 5V cathode materials for lithium-ion batteries. *ChemPlusChem* 78:636
- Jin GH, Qiao H, Xie HL, Wang HY et al (2014) Electrospinning: designed architectures for energy conversion and storage devices. *Electrochim Acta* 150:1
- Min JW, Yim CJ, Im WB (2013) Facile synthesis of electrospun  $\text{Li}_{1.2}\text{Ni}_{0.17}\text{Co}_{0.17}\text{Mn}_{0.5}\text{O}_2$  nanofiber and its enhanced high-rate performance for lithium-ion battery applications. *ACS Appl. Mater. Interfaces* 5:7765

31. Lee MJ, Lee S, Oh P, Kim Y, Cho J (2014) High performance  $\text{LiMn}_2\text{O}_4$  cathode materials grown with epitaxial layered nanostructure for Li-ion batteries. *Nano Lett.* 14:993
32. Wang JX, Zhang QB, Li XH, Wang ZX, Guo HJ, Xu DG, Zhang KL (2014) Sputtering graphite coating to improve the elevated-temperature cycling ability of the  $\text{LiMn}_2\text{O}_4$  electrode. *Phys Chem Chem Phys* 16:16021

**Submit your manuscript to a SpringerOpen<sup>®</sup> journal and benefit from:**

- Convenient online submission
- Rigorous peer review
- Immediate publication on acceptance
- Open access: articles freely available online
- High visibility within the field
- Retaining the copyright to your article

---

Submit your next manuscript at ► [springeropen.com](http://springeropen.com)

---